We are IntechOpen,
the world's leading publisher of
Open Access books
Built by scientists, for scientists

4,400
Open access books available

117,000
International authors and editors

130M
Downloads

Our authors are among the

154
Countries delivered to

TOP 1%
most cited scientists

12.2%
Contributors from top 500 universities

CLARIVATE ANALYTICS

BOOK CITATION INDEX

INDEXED

WEB OF SCIENCE™

Selection of our books indexed in the Book Citation Index
in Web of Science™ Core Collection (BKCI)

Interested in publishing with us?
Contact book.department@intechopen.com

Multi-Beam Multi-Target Pulsed Laser Deposition of AZO Films with Polymer Nanoparticles for Thermoelectric Energy Harvesters

Abdalla M. Darwish, Sergey S. Sarkisov,
Paolo Mele and Shrikant Saini

Additional information is available at the end of the chapter

Abstract

In comparison with metallic thermoelectric films, oxide films with artificial nanodefects have been seldom studied. And there has been no report on the incorporation of island-shaped organic nanoparticles. We describe a new approach to introduce nanometer-sized phonon scatterers in aluminum-doped ZnO (AZO) thermoelectric thin films–concurrent multi-beam multi-target-pulsed laser deposition and the matrix-assisted pulsed laser evaporation (MBMT-PLD/MAPLE). The approach was used to make nanocomposite thin films of AZO matrix with evenly dispersed poly(methyl methacrylate) (PMMA) nanoparticles. The introduction of the nanoparticles enhanced phonon scattering with consequent decrease of thermal conductivity by 20%. The electrical conductivity did not decrease after the addition of the second phase, as it would be predicted by Wiedemann-Franz law, but improved by 350% over pure AZO film. The thermoelectric figure of merit of the nanocomposite film became twice that of the pure AZO film. Taking advantage of room-temperature deposition, optimized AZO nanocomposite films are expected to be used in real applications, such as thin film modules deposited on flexible polymeric substrates for ubiquitous harvesting of the waste heat.

Keywords: laser ablation, pulsed laser deposition, matrix-assisted pulsed laser evaporation, nanocomposite films, AZO, polymer nanoparticles, thermos-electric energy harvesters

1. Introduction

ZnO is a well-known *n*-type semiconductor used in a variety of applications such as optical devices, piezoelectric transducers, transparent electrodes, and gas sensors [1]. Furthermore, interesting results have been published on Al-doped ZnO (AZO) as a sustainable thermoelectric

material to replace toxic and expensive materials based on Se, Te, and Bi [2]. More recently, researchers have focused on the preparation of AZO in thin film form due to the possibility to control better the morphology and crystalline orientation of the films. In pure AZO films prepared by the conventional pulsed laser deposition (PLD) on single crystal substrates at relatively low temperatures (400–600°C), the thermal conductivity κ has been reduced significantly with respect to the bulk material due to the enhanced phonon scattering at the film substrate interface and at grain boundaries [3]. Ultimately, this approach has yielded a higher thermoelectric figure of merit, ZT [4]. Further improvement of ZT can be achieved by the introduction of multilayer structures and nanodefects acting as additional phonon scatterers reducing the thermal conductivity [5, 6].

In contrast to metallic thermoelectric films, oxide films with artificial nanodefects have been seldom studied: $SrTiO_3/Nb\text{-}SrTiO_3$ [7], AZO/hydroquinone [8], and AZO/Y_2O_3 [9]. There is still no report on oxide films with nanodefects in the form of polymer nanoparticles. This chapter describes nanocomposite thin films made of AZO matrix with evenly dispersed poly (methyl methacrylate) (PMMA) nanoparticles produced by the concurrent multi-beam multi-target pulsed laser deposition of AZO and matrix-assisted pulsed laser evaporation of the polymer (MBMT-PLD/MAPLE) [10–13].

A wide variety of nanocomposite materials based on polymers and inorganic substances can be classified as "polymer nanocomposites," where the polymer serves as a host for inorganic nanoparticles [14, 15]. In case, when the volume fraction of the polymer decreased below 90% (and the interaction between the inorganic inclusions became stronger, as illustrated in **Figures 1** and **2**), the resulting materials were often called as "organic-inorganic hybrid composites" [14]. In some occasions, one polymer was used as a host for a nanoparticles made of
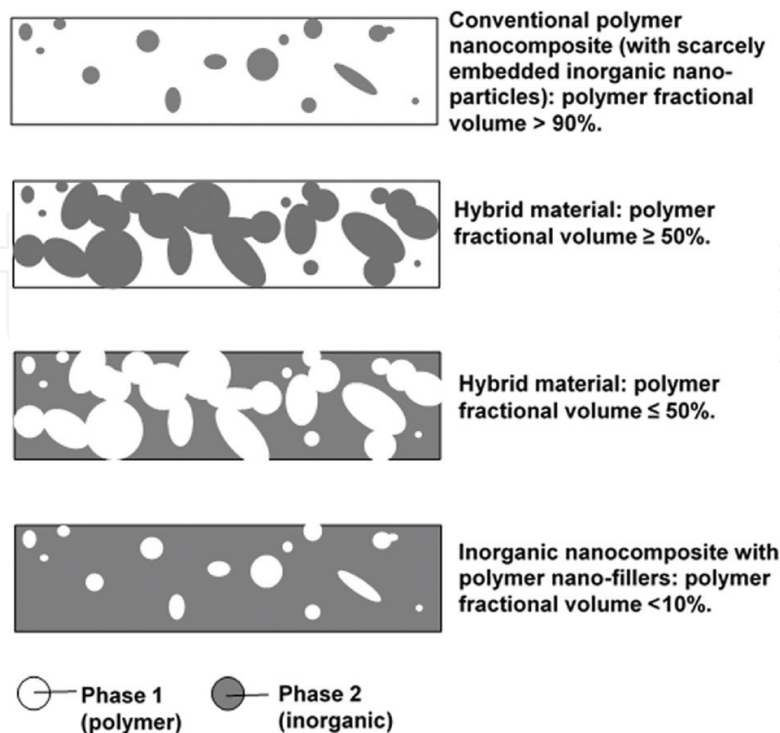

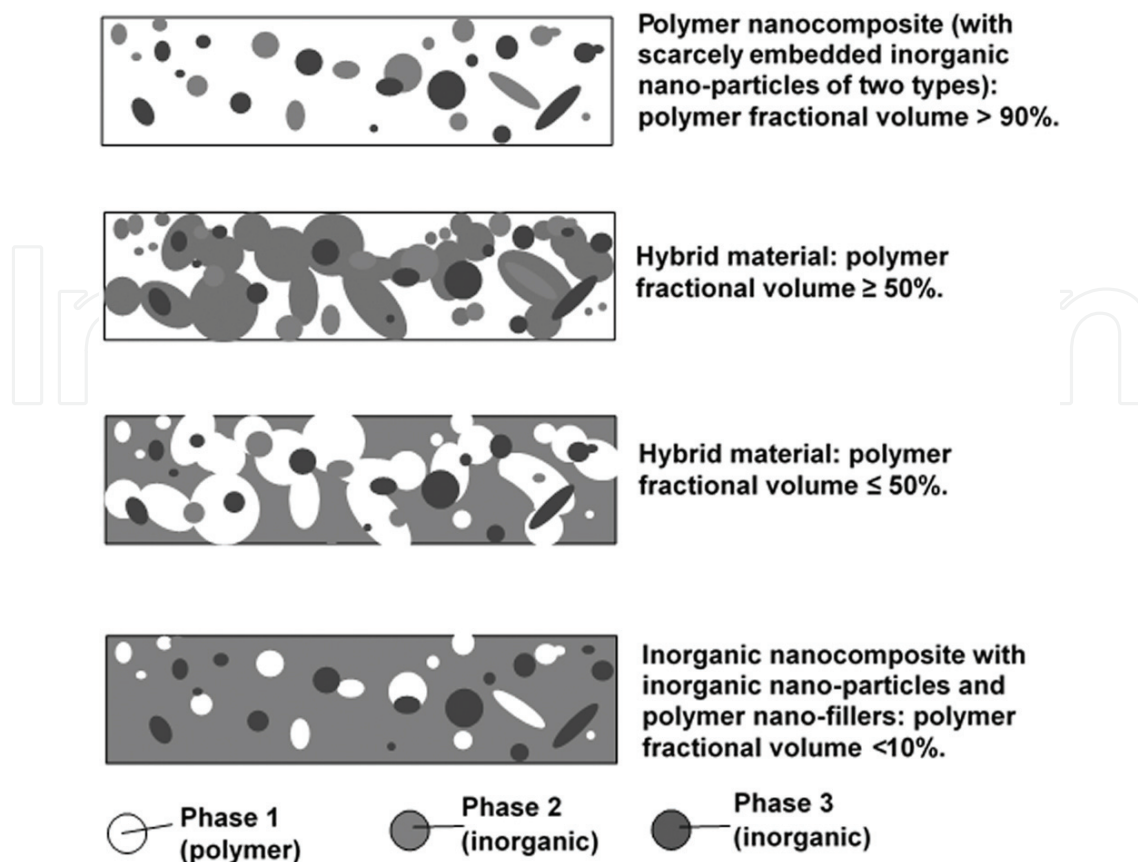**Figure 1.** Two-phase polymer-inorganic nanocomposite films.

Figure 2. Three-phase polymer-inorganic nanocomposite films.

another polymer [16]. Making a uniformly mixed nanocomposite films with low fractional volume (<10%) of the polymer and at least one inorganic phase prevailing and serving as a host for the polymer nanoparticles (**Figures 1** and **2**) has remained an unachievable goal because the list of suitable technologies was limited mainly to the sol-gel process [17]. Hence, the two novelty features of this work are: (i) the use of MBMT-PLD/MAPLE to produce an oxide-polymer nanocomposite film at room temperature with the oxide acting as a host to the polymer nanoparticles and (ii) the use of the polymer nanoparticles as phonon scatterers. The description given below demonstrates how the approach improves the thermoelectric properties of AZO films.

2. Methods and materials

The MBMT-PLD/MAPLE system at Dillard University is schematically presented in **Figure 3**. Two pulsed laser beams ablated concurrently two targets and ejected the target materials in the plumes that propagated toward the surface of a substrate where they mixed and formed a nanocomposite film. Linear actuators tilted the targets and changed the directions of the plumes in order to secure uniform mixing of the target materials in the film. Plume 1 is formed by laser beam 1 ablating a conventional solid inorganic PLD target. The second target (to the right) was a polymer solution frozen by circulating liquid nitrogen (LN). Accordingly, the process of polymer deposition was the matrix-assisted pulsed laser evaporation (MAPLE) [10–13]. All the
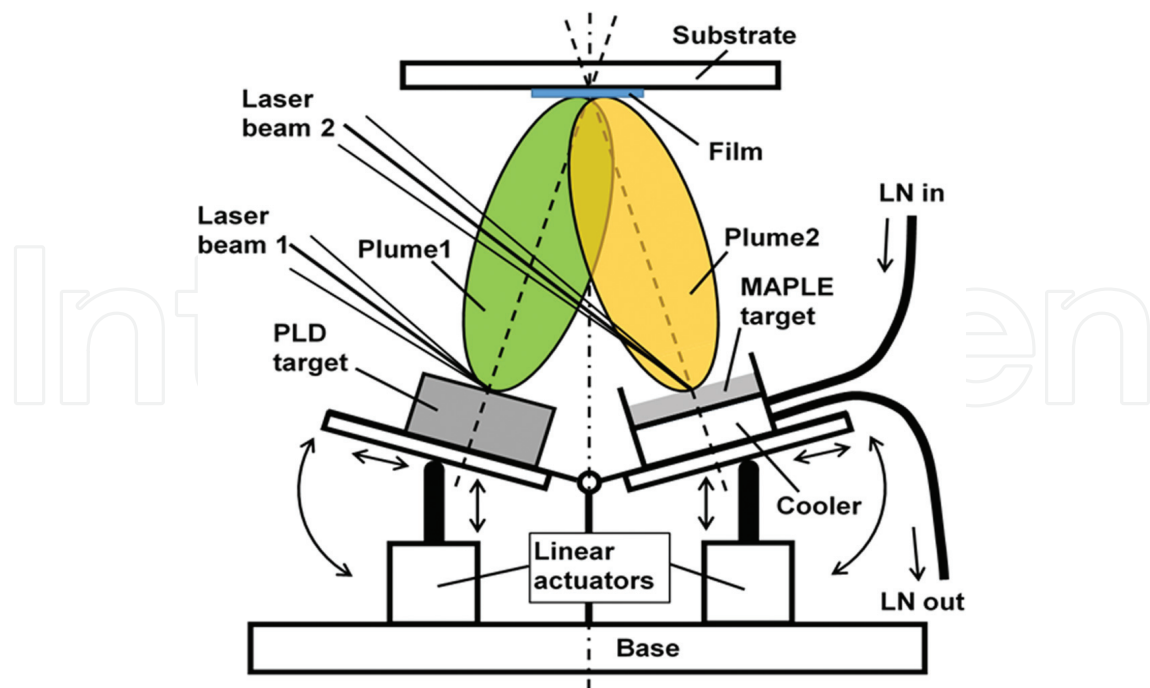
Figure 3. The schematic of the multi-beam multi-target-pulsed laser deposition system used to make the films.

components of the deposition system were placed in a vacuum chamber (not shown) with optical windows for the laser beams. The inorganic, AZO target was a pellet of $Zn_{0.98}Al_{0.02}O$ where the aluminum fraction was 2% of the total by weight as compared with zinc, not counting the oxygen. The AZO pellet had 20 mm in diameter and 3 mm in thickness. The pellet was prepared by the spark plasma sintering method as described elsewhere [18]. The MAPLE target was a solution of PMMA in chlorobenzene at a proportion of 1 g solids per 10 mL liquids filtered with 0.2 μm filter. The solution was poured in a copper cup of the MAPLE target assembly (**Figure 3**) and frozen in liquid nitrogen (LN). The laser source was a Spectra Physics Quanta Ray Nd:YAG Q-switched Pro-250-50 laser with a pulse repetition rate of 50 Hz, 750 mJ energy per pulse at the 1064 nm fundamental wavelength, and 400 mJ energy per pulse at the 532 nm second harmonic. The AZO target was ablated with the 532 nm beam. The fluence was tuned up between 0.8 and 1.0 J/cm^2 per pulse. The MAPLE target was evaporated with the 1064 nm beam. The fluence was ranging from 0.84 to 2.4 J/cm^2 per pulse to maintain a volume fraction of PMMA in the AZO matrix of about 5%. The deposition time was 3.0 min. The thickness of the deposited films was approximately 150 nm as measured with an atomic force microscope. The films were deposited on Al_2O_3 (sapphire) (100) single crystal substrates at room temperature in vacuum. The inorganic target was rotated during the irradiation of laser beam. The substrate-target distance was maintained about 35 mm. Deposition of pure AZO films in the same experimental conditions was carried out in order to have reference samples.

3. Results and discussion

X-ray diffraction (XRD) analysis of the as-grown AZO-PMMA films conducted with a Bruker D2 Phaser diffractometer (**Figure 4**) revealed the presence of polycrystalline AZO, while peaks
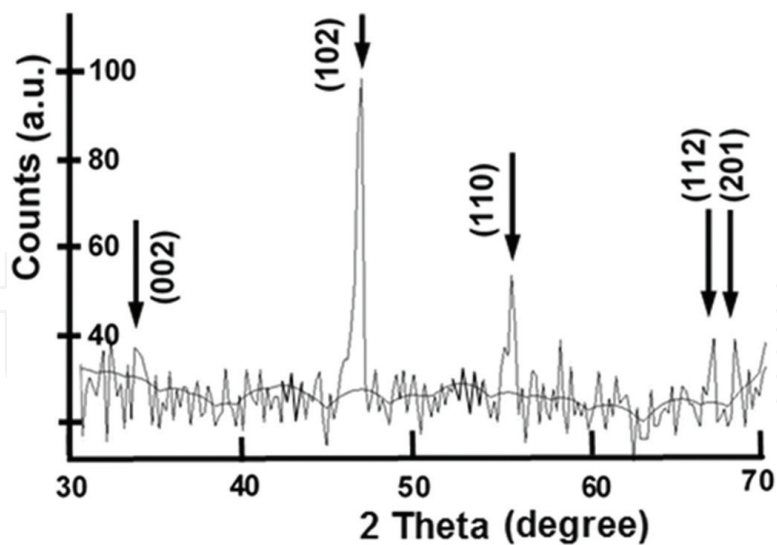
Figure 4. X-ray diffraction spectrum of the films (peaks are indexed with [*hkl*] reflections of AZO matrix).
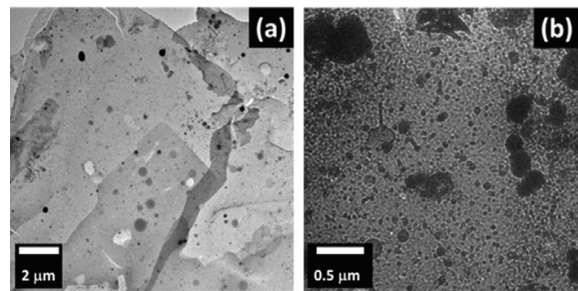

Figure 5. Top-view TEM images of the films deposited on Al_2O_3 substrate with (a) low and (b) high magnification.

of PMMA were absent. Polycrystallinity of AZO is due to the fact that the ablation in MBMT-PLD/MAPLE system was performed at room temperature to solidify PMMA after its condensation on the substrate (PMMA has been reported to melt at about 430 K [19]). As widely observed in literature, AZO films deposited at room temperature by conventional PLD are commonly polycrystalline [20–22].

Figure 5 (a) and **(b)** present TEM images of the film samples that were peeled off from the Al_2O_3 substrate. Typically, polymer nanoparticles-nanoclusters of a size of 10–50 nm are seen embedded in the AZO matrix. The formation of the nanoclusters is due to the heavy entanglement of the polymer molecules ruled by chemical interactions during their condensation on the substrates and chemical interaction with the ceramic host. Some polymer molecules could also self-assemble in individual fibers creating networks across the AZO matrix.

The electrical conductivity versus temperature ($\sigma - T$) characteristics of the films were measured by the conventional four-probe technique, and Seebeck coefficient was measured by a commercial system (from MMR technologies) in the temperature range from 300 to 600 K. Further, the thermal conductivity κ of the films was measured at 300 K using the time domain thermoreflectance (TDTR) technique [23, 24].

Sample	Electrical conductivity σ (S/cm) (300K/600K)		Seebeck coefficient S (μV/K) (300K/600K)		Power factor σS^2 (mW/(m.K^2)) (300K/600K)		Thermal conductivity κ (Wm^{-1}K^{-1}) 300K		ZT (300K/600K)	
	Pure AZO	AZO + PMMA	Pure AZO	AZO + PMMA	Pure AZO	AZO + PMMA	Pure AZO	AZO + PMMA	Pure AZO	AZO + PMMA
Film on Al$_2$O$_3$	433/539	1382/1630	−15/−30	−9/−20	0.01/0.05	0.01/0.07	7.4 ± 0.2	5.9 ± 0.3	0.005/0.04	0.0055/0.07
Bulk AZO	206/152		−132/−150		0.35/0.34		34		0.0035/0.014	

Table 1. Comparative performance of the nanocomposite thermoelectric AZO-PMMA films.

Electro-conductive and thermo-electrical characteristics of the AZO-PMMA nanocomposite films in the range of 300–600 K are presented in **Figures 6** through 11 and **Table 1**. Performance of pure AZO films deposited on the same substrate is also reported for comparison.

Electrical conductivity σ of AZO + PMMA films is higher than that of the AZO films over all the measured temperature range and increases with the increase of temperature (**Figure 6**). The highest value of the electrical conductivity is 1630 S/cm at 600 K, three times increase comparing to pure AZO films. 1 S/cm (siemens per centimeter) is 100 times 1 S/m, the unit of electrical conductivity in SI, 1 S/m = 1 (A^2.s^3)/(kg.m^3). The significant increase of σ can be explained as follows. At first, as long as PMMA remains unaffected by the temperatures applied during the measurement (below 430 K), the polymer can be assumed to increase the number of oxygen vacancies in AZO usually resulting in the increase of electrical conductivity in a hybrid system. Another scenario is that above 430 K, PMMA decomposes in CO$_2$ and by-products. Then, carbon dioxide converts into amorphous carbon, which is known to have good electrical conductivity (around 670 S/cm [25]). Since, virgin PMMA has very low electrical
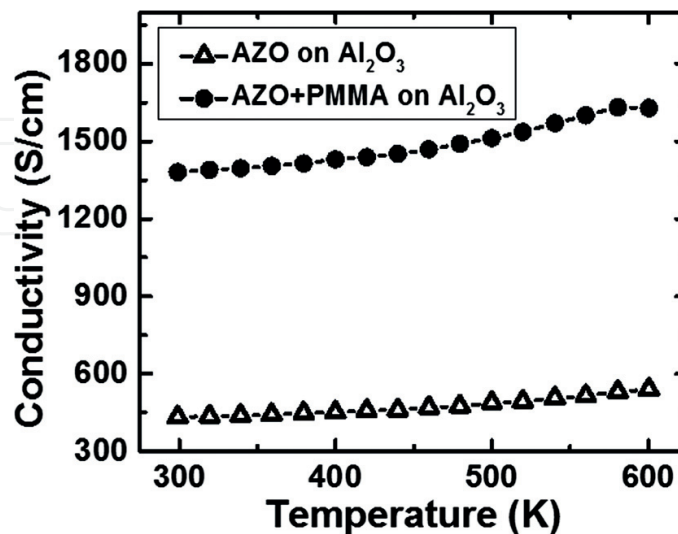

Figure 6. Temperature dependence of the electrical conductivity of AZO and AZO + PMMA films deposited on Al$_2$O$_3$ substrates.
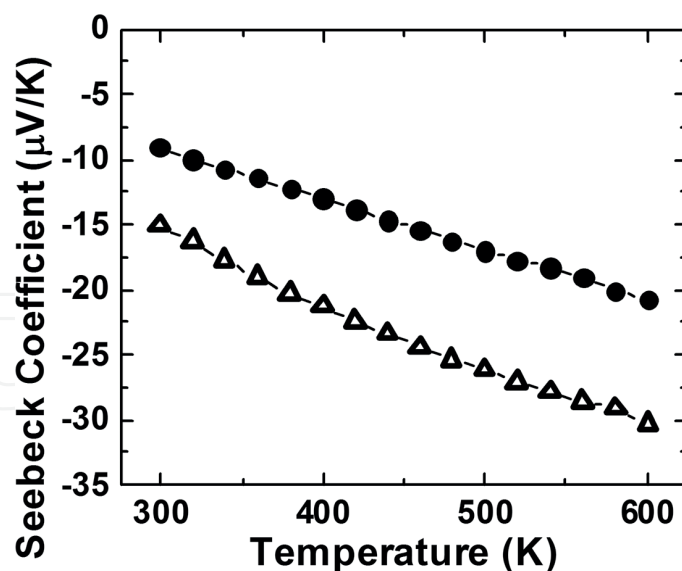
Figure 7. Temperature dependence of Seebeck coefficient of AZO and AZO + PMMA thin films on Al_2O_3 substrates. Symbols used to represent data points are the same as in **Figure 6**.

conductivity (of the order of 10^{-13} S/cm [26]), the degree of polymer conversion into carbon could be assumed rather substantially, and thus, affecting not only σ, but other physical properties that were becoming similar to those of an AZO-carbon nanocomposite.

Seebeck coefficient versus temperature plot is presented in **Figure 7**. The negative sign of Seebeck coefficient indicates electrons as the electric charge carriers and correspondingly the hybrid composite material being an *n*-type semiconductor. The magnitude of Seebeck coefficient increases with the temperature increase. Overall, the magnitude of Seebeck coefficient of AZO + PMMA hybrid films is lower than that of the pure AZO thin film due to the fact that it has more electric charge carriers. The highest absolute value of Seebeck coefficient is about -30 μV/K at 600 K for AZO thin films. Based on the measured electrical conductivity and Seebeck coefficient, power factor $PF = \sigma S^2$ was calculated. The value of *PF* for AZO + PMMA films (**Figure 8**) was found to be higher than that of the AZO thin films due to the higher electrical conductivity. The maximum value of *PF* is about 0.07 mW/(m.K^2) at 600 K.

Electrical conduction is governed by thermally activated hopping mechanism as is indicated by linear plot of $\ln(\sigma T)$ versus $1/T$ in **Figure 9**. The electrical conductivity follows relation $\sigma T = A \exp[-E_\sigma/(k_b T)]$ (where E_σ is the activation energy for electrical conductivity, A is the pre-exponential factor, k_B is the Boltzmann constant) [27]. Activation energy E_σ was calculated using the slope of the linear fit of the plots to be about 44 and 47 meV for AZO + PMMA and AZO films respectively. Slightly lower activation energy of the nanocomposite film indicates that the charge carriers with lower energy hopping between the grain boundaries also participate in electrical conduction. Due to this, AZO + PMMA film exhibits higher electrical conductivity. Further, the temperature dependence of Seebeck coefficient can be described as $S = (k_B/e)[E_S/(k_B T) + B]$, where E_S is the thermopower activation energy and B is the heat of transport taken as temperature independent [27]. Activation energy E_S was calculated from the slope of linear fitting of the plots of S versus $1/T$ (**Figure 10**) to be 7.0–9.2 meV for AZO + PMMA and
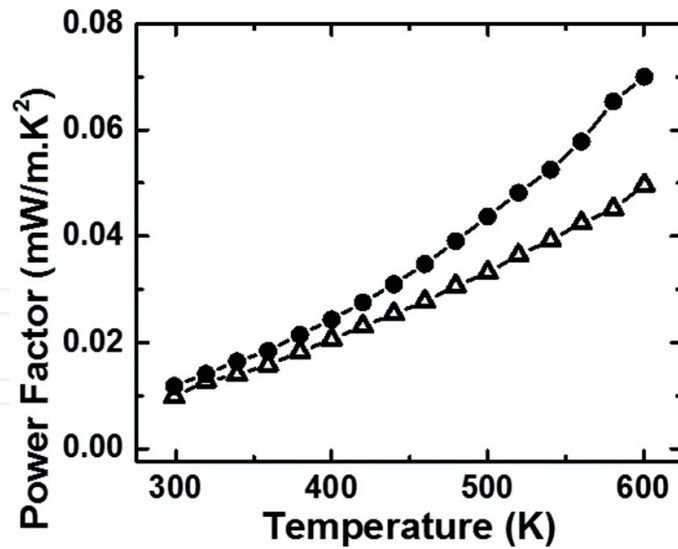
Figure 8. Temperature dependence of the power factor of AZO and AZO + PMMA thin films on Al_2O_3 substrates. Symbols used to represent data points are the same as in **Figure 6**.
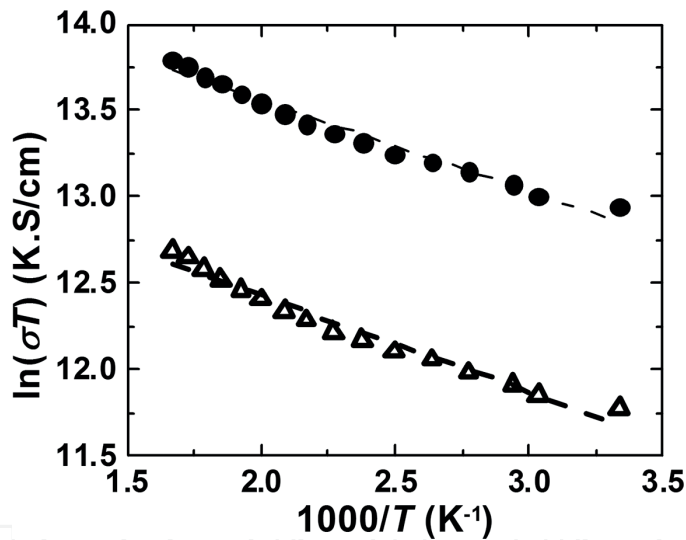

Figure 9. Inverse temperature dependence of $\ln(\sigma T)$ of AZO and AZO + PMMA thin films on Al_2O_3 substrate. Dashed lines are the linear fit of the corresponding plots. Symbols used to represent data points for different samples as in **Figure 6**.

AZO films, respectively. The values of E_σ are about five to six times greater than E_S, which suggests that a part of the activation energy is arising from the activated mobility of the small polaron, which does not contribute to thermopower and the formation of which has been reported for a number of oxides [27, 28]. It is worth of mentioning that, besides the thermal hopping mechanisms, the temperature-independent tunneling electron transport mechanism can be sometimes observed in the granulated multi-component films prepared by PLD as it has been recently reported (for the films made of gold and silver nanogranules at a temperature below 60°C) in paper [29].
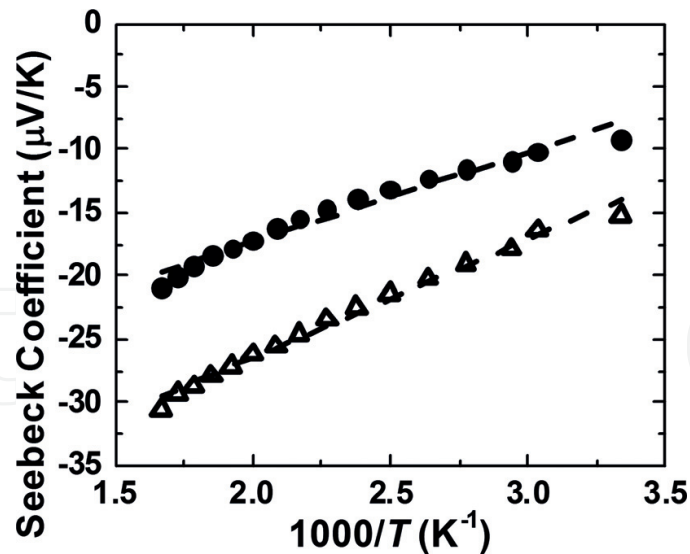
Figure 10. Inverse temperature dependence of Seebeck coefficient of AZO and AZO + PMMA films on Al_2O_3 substrates. Dashed lines are the linear fit of the corresponding plots. Symbols used to represent data points for different samples are the same as in **Figure 6**.

Thermal conductivity κ (at 300 K) was measured by the above-described TDTR method to be (5.9 ± 0.3) and (7.4 ± 0.2) W/m.K for AZO + PMMA and AZO film, respectively. Less κ for the hybrid film can be attributed to two factors: low thermal conductivity of PMMA ($\kappa = 0.25$ W/m. K at room temperature [30]) and the phonon scattering from uniformly dispersed PMMA nanoparticles (as shown in **Figure 3**). These out-of-plane film thermal conductivity values $\kappa(300K)$ measured at 300 K were further used in calculating the thermoelectric figure of merit $ZT = \sigma S^2 T/\kappa'(T)$ in the range of 300–600 K, where $\kappa'(T)$ is the film in-plane thermal conductivity at a given temperature T. For elevated temperatures ($T > 300$ K), the replacement of $\kappa'(T)$ by $\kappa(300K)$ can be validated by two facts: (i) in ZnO films, the in-plane thermal conductivity determined at different conditions was always higher than the out-of-plane one [31]; and (ii) the thermal conductivity of ZnO films was found to decrease with increasing temperature [32]. So, the replacement will not change the trend of ZT growth with T. **Figure 11** and **Table 1** show that ZT for AZO + PMMA film is always greater than that of the pure AZO film (twice as great at 600 K). This is due to the higher electrical conductivity and lower thermal conductivity of the nanocomposite film.

The electrical conductivity σ of AZO + PMMA films turned out to violate the Wiedemann-Franz law, $\kappa_{el}/\sigma = L_0 T$ (κ_{el} is the electronic component of the combined thermal conductivity $\kappa = \kappa_{ph} + \kappa_{el}$, κ_{ph} is the phonon component, L_0 is the Lorentz number) and got decoupled from the thermal conductivity, a common feature of complex and disordered media (so called "electron crystals and phonon glasses") [33]. The hypothetical structure of the composite AZO + PMMA medium can be schematically depicted in **Figure 12**. The polymer phase in the inorganic AZO matrix is assumed to be present in a variety of forms: nanoclusters (nanoparticles or nanodots), nanofibers, and fiber nanobundles. Nanoclusters are formed by the entangled long-chain polymer molecules. Nanofibers may be formed by straightened single polymer strands or the bundles of parallel polymer strands. All these formations (nanoclusters,
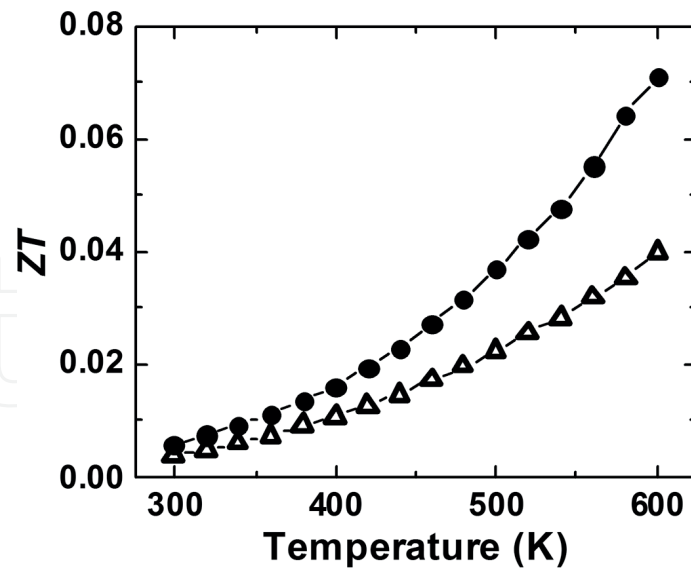
Figure 11. Temperature dependence of the thermoelectric figure of merit ZT of AZO and AZO + PMMA thin films on Al_2O_3 substrates. Symbols used to represent data points are the same as in **Figure 6**. ZT was calculated using the thermal conductivities of AZO and AZO + PMMA films on Al_2O_3 substrates measured at 300 K (see **Table 1**).
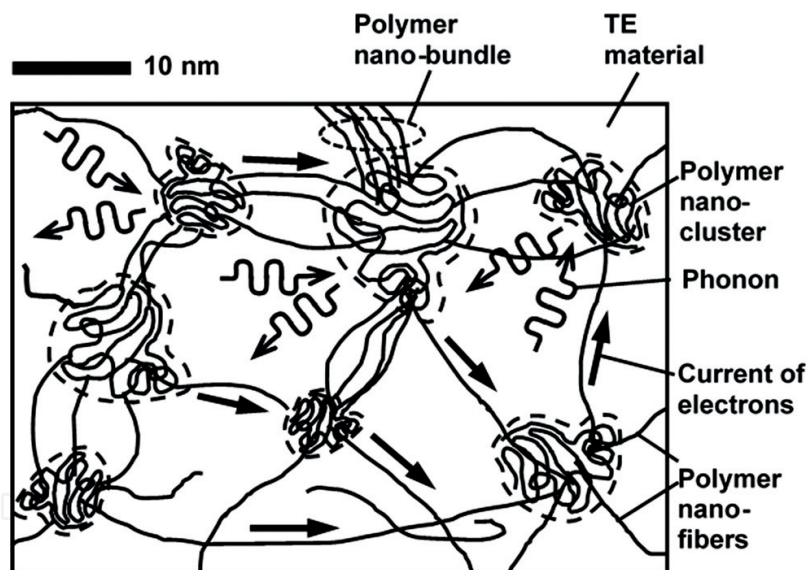

Figure 12. Schematic diagram of the AZO + PMMA nanocomposite film illustrating the effects of the polymer nanophase on the electrical and thermal conductivity of the AZO host.

nanofibers, and nanobundles) can be interconnected forming a network across the inorganic host. The polymer nanoclusters increased phonon scattering and reduced thermal conductivity of the nanocomposite films.

As was mentioned above, one of the mechanisms of significant (three times) increase of the electrical conductivity of AZO + PMMA films with respect to pure AZO could be the carbonization of the polymer phase. Carbonization occurs as a pyrolysis–a thermochemical decomposition of organic material at elevated temperatures without oxygen (or any halogen).

It involves the simultaneous change of chemical composition and physical phase. Pyrolysis is a type of thermolysis, and is most commonly observed in organic materials exposed to elevated temperatures. It is one of the processes involved in charring wood, starting at 200–300°C (390–570°F). It also occurs in fires where solid fuels are burning or when vegetation comes into contact with lava in volcanic eruptions. In general, pyrolysis of organic substances produces gas and liquid products and leaves a solid residue richer in carbon content, char. Pyrolysis leading to carbonization of polymers, such as PMMA, poly(vinylidene fluoride)—PVDF, poly (acrylonitrile)—PAN, and poly-N-vinylformamide—PNVF, during laser ablation and heat treatment has been reported before and used to modify the electrical conductivity of polymer coatings and fibers [34–36]. In case of AZO + PMMA films, carbonization could turn the network of the polymer nanoclusters and nanofibers into an additional efficient passage for the electric current (**Figure 12**) contributing to the overall increase of the electrical conductivity of the nanocomposite films and eventually to the increase of *ZT*.

4. Conclusions

The new concurrent MBMT-PLD/MAPLE deposition method has been successfully used to produce nanocomposite oxide-polymer thermoelectric films composed of AZO matrix with uniformly dispersed PMMA nanoparticles. The deposition was conducted at room temperature and on the cold (kept also at room temperature) substrate with no buffer gas. The volume fraction of the polymer material in the AZO matrix was chosen to be around 5%. These deposition conditions affected favorably the enhancement of the thermoelectric effect because the long-chain polymer molecules had a better chance to reach the substrate and mix with the inorganic matrix material without being decomposed. The chosen polymer fraction was small enough not to compromise substantially the electrical conductivity of the matrix. The PMMA nanoparticles allowed enhancing the phonon scattering with consequent decrease of thermal conductivity as compared to pure AZO film. The electrical conductivity did not drop after the addition of the second phase, as it would be expected from Wiedemann-Franz law, but grew three times higher over pure AZO film. This was assumingly due to the increase of the number of oxygen vacancies in AZO caused by PMMA or/and by the polymer carbonization at elevated temperatures. The thermoelectric figure of merit was improved by a factor of two. Further experiments would be necessary to establish the optimal proportion of the polymer nanoadditive in AZO matrix and other deposition parameters that maximize the thermoelectric performance of the nanocomposite films. Taking advantage of room-temperature deposition, optimized AZO nanocomposite films are expected to be used in real applications such as thin film modules deposited on flexible polymer substrates for ubiquitous harvesting of the waste heat.

Acknowledgements

Author details

Abdalla M. Darwish[1]*, Sergey S. Sarkisov[2], Paolo Mele[3] and Shrikant Saini[3]

*Address all correspondence to: adarwish@bellsouth.net

1 Dillard University, New Orleans, USA

2 SSS Optical Technologies LLC, Huntsville, USA

3 Muroran Institute of Technology, Muroran, Japan

References

[1] Ozgür U, Alivov YI, Liu C, Teke A, Reschikov MA, Dögan S, et al. A comprehensive review of ZnO materials and devices. Journal of Applied Physics. 2005;**98**(4):103/041301. DOI: 10.1063/1.1992666

[2] Ohtaki M, Tsubota T, Eguchi K, Arai H. High-temperature thermoelectric properties of $(Zn_{1-x}Al_x)O$. Journal of Applied Physics. 1996;**79**:1816

[3] Mele P, Saini S, Honda H, Matsumoto K, Miyazaki K, Hagino H, et al. Effect of substrate on thermoelectric properties of Al-doped ZnO thin films. Applied Physics Letters. 2013;**102**:253903

[4] Saini S, Mele P, Honda H, Suzuki T, Matsumoto K, Miyazaki K, et al. Effect of self-grown seed layer on thermoelectric properties of ZnO thin films. Thin Solid Films. 2016;**605**:289-294

[5] Hicks LD, Dresselhaus MMS. Effect of quantum-well structures on the thermoelectric figure of merit. Physical Review B. 1993;**47**:12727

[6] Venkatasubramanian R, Siivola E, Colpitts T, O'Quinn B. Thin-film thermoelectric devices with high room-temperature figure of merit. Nature. 2001;**413**:597-602

[7] Ohta H, Kim SW, Mune Y, Mizoguchi T, Nomura K, Ohta S, et al. Giant thermoelectric Seebeck coefficient of a two-dimensional electron gas in $SrTiO_3$. Nature Materials. 2007;**6**:129-134

[8] Tynell T, Giri A, Gaskins J, Hopkins PE, Mele P, Miyazaki K, et al. Efficiently suppressed thermal conductivity in ZnO thin films via periodic introduction of organic layers. Journal of Materials Chemistry A. 2014;**2**:12150

[9] Mele P, Saini S, Tiwari A, Hopkins PE, Miyazaki K, Ichinose A, et al. Thermoelectric and structural characterization of Al-doped ZnO/Y_2O_3 multilayers. Journal of Nanoscience and Nanotechnology. 2017;**17**:1616

[10] Darwish AM, Sagapolutele MT, Sarkisov S, Patel D, Hui D, Koplitz B. Double beam pulsed laser deposition of composite films of poly(methyl methacrylate) and rare earth fluoride upconversion phosphors. Composites B. 2013;**55**:139-146

[11] Darwish AM, Burkett A, Blackwell A, Taylor K, Sarkisov S, Patel D, et al. Polymer-inorganic nano-composite thin film upconversion light emitters prepared by double-beam matrix assisted pulsed laser evaporation (DB-MAPLE) method. Composites B. 2015;**68**:355-364

[12] Darwish AM, Wilson S, Blackwell A, Taylor K, Sarkisov SS, Patel DN, et al. Ammonia sensor based on polymer-inorganic nano-composite thin film upconversion light emitter prepared by double-beam pulsed laser deposition. American Journal of Materials Science. 2015;**5**:8-15

[13] Darwish AM, Moore S, Mohammad A, Alexander D, Bastian T, Sarkisov S, et al. Polymer nano-composite films with inorganic upconversion phosphor and electro-optic additives made by concurrent triple-beam matrix assisted and direct pulsed laser deposition. Composites B. 2017;**109**:82-90

[14] Gross S, Camozzo D, Di Noto V, Armelao L, Tondello E. PMMA: A key macromolecular component for dielectric low-κ hybrid inorganic–organic polymer films. European Polymer Journal. 2007;**43**:673-696

[15] Marquis DM, Guillaume É, Chivas-Joly C. Properties of Nanofillers in polymer. In: Nanocomposites and Polymers with Analytical Methods. Rijeka, Croatia: InTech; 2011

[16] Abdollahi M, Alboofetileh M, Rezaeia M, Behroozb R. Comparing physico-mechanical and thermal properties of alginate nanocomposite films reinforced with organic and/or inorganic nanofillers. Food Hydrocolloids. 2013;**32**:416-424

[17] Ishchenko SS, Budnitskaya VL, Lebedev EV, Kozak NV. Hybrid composites based on organic-inorganic sol-gel systems. Russian Journal of Applied Chemistry. 2011;**84**:1952-1957

[18] Mele P, Kamei H, Yasumune H, Kaname H, Miyazaki K. Development of thermoelectric module based on dense $Ca_3Co_4O_9$ and $Zn_{0.98}Al_{0.02}O$ legs. Metals and Materials International. 2014;**20**(2):389-397

[19] Smith WF, Hashemi J. Foundations of Materials Science and Engineering. New York: McGraw-Hill; 2006. p. 509

[20] Sun Y, Maemoto T, Sasa S. Future of electron devices, Kansai (IMFEDK). In: Proceedings of 2014 IEEE International Meeting for Future of Electron Devices; 19–20 June 2014; Kansai, Kyoto, Japan. IEEE; 2014

[21] Liu Y, Zhao L, Lian J. Al-doped ZnO films by pulsed laser deposition at room temperature. Vacuum. 2006;**81**:18-21

[22] Gondoni P, Mazzolini P, Russo V, Diani M, Amati M, Gregoratti L, et al. Tuning electrical properties of hierarchically assembled Al-doped ZnO nanoforests by room temperature pulsed laser deposition. Thin Solid Films. 2015;**594**:12-17

[23] Schmidt J, Chen X, Chen G. Pulse accumulation, radial heat conduction, and anisotropic thermal conductivity in pump-probe transient thermoreflectance. The Review of Scientific Instruments. 2008;**79**:114902

[24] Yada S, Oyake T, Sakata M, Shiomi J. Filler-depletion layer adjacent to interface impacts performance of thermal interface material. AIP Advances. 2016;**6**:015117

[25] Serway RA, Faugh JS. College Physics. 6th ed. Belmont, CA: Thomson; 2003

[26] Hussien B. The D.C and A.C. electrical properties of PMMA-Al_2O_3 composites. The European Journal of Scientific Research. 2011;**52**:236-242

[27] Ponnambalam V, Varadaraju UV. Observation of variable-range hopping up to 900 K in the $YLa_xBa_2 - xCu_3O_7 - \delta$ system. Physical Review B. 1995;**52**:16213

[28] Cutler M, Mott F. Observation of Anderson localization in an electron gas. Physics Review. 1969;**181**:1336-1340

[29] Kavokin A, Kutrovskaya S, Kucherik A, Osipov A, Vartanyn T, Arakelyn S. The crossover between tunnel and hopping conductivity in granulated films of noble metals. Superlattices and Microstructures. In Press, Corrected Proof. Available online 19 June 2017;1-5

[30] Assaael MJ, Antoniadis KD, Wu J. New measurements of the thermal conductivity of PMMA, BK7, and Pyrex 7740 up to 450K. International Journal of Thermophysics. 2008; **29**:1257-1266

[31] Xu Y, Goto M, Rato R, Tanaka Y, Kagawa Y. Thermal conductivity of ZnO thin film produced by reactive sputtering. Journal of Applied Physics. 2012;**111**:084320

[32] Alvarez-Quintana J, Martinez E, Perez-Tijerina E, Perez-Garcia SA, Rodriguez-Vejo J. Temperature dependent thermal conductivity of polycrystalline ZnO films. Journal of Applied Physics. 2010;**107**:063713

[33] Wikipedia. Wiedemann–Franz law [Internet]. [Updated: 2-July-2017]. Available from: https://en.wikipedia.org/wiki/WiedemannFranz_law [Accessed: 6-July-2017]

[34] Blancet GB, Fincher CR Jr. Laser induced unzipping: A thermal route to polymer ablation. Applied Physics Letters. 1994;**65**(10):1311-1313

[35] Morita N, Shimotsuma Y, Nishi M, Sakakura M, Miura K, Hirao K. Direct micro carbonization inside polymer using focused femtosecond laser pulses. Applied Physics Letters. 2014;**105**:201104

[36] Molenda M, Swietoslawski M, Drozdek M, Dudek B, Dziembaj R. Morphology and electric conductivity of carbon nanocoatings prepared from pyrolized polymers. Journal of Nanomaterials. 2014;**2014**:7/103418